Naval Research Laboratory
Washington, DC 20375-5320

NRL/7320/MR—2023/10

Cool-Skin and Warm-Layer Corrections to Sea Surface Temperature in NCOM

JIE YU

TOMMY G. JENSEN

TIMOTHY J. CAMPBELL

Nearshore and Coupled Model Systems Section
Ocean Sciences Division

DAVID D. FLAGG

Mesoscale Modeling Section
Marine Meteorology Division

November 13, 2023

REPORT DOCUMENTATION PAGE

Form Approved
OMB No. 0704-0188

1. REPORT DATE *(DD-MM-YYYY)*	**2. REPORT TYPE**	**3. DATES COVERED** *(From - To)*
13-11-2023	NRL Memorandum Report	

4. TITLE AND SUBTITLE

Cool-Skin and Warm-Layer Corrections to Sea Surface Temperature in NCOM

5a. CONTRACT NUMBER

5b. GRANT NUMBER

5c. PROGRAM ELEMENT NUMBER

6. AUTHOR(S)

Jie Yu, Tommy G. Jensen, David D. Flagg, and Timothy J. Campbell

5d. PROJECT NUMBER

5e. TASK NUMBER

5f. WORK UNIT NUMBER
6C02

7. PERFORMING ORGANIZATION NAME(S) AND ADDRESS(ES)

Naval Research Laboratory
4555 Overlook Avenue, SW
Washington, DC 20375-5320

8. PERFORMING ORGANIZATION REPORT NUMBER

NRL/7320/MR--2023/10

9. SPONSORING / MONITORING AGENCY NAME(S) AND ADDRESS(ES)

Office of Naval Research
One Liberty Center
875 N. Randolph Street, Suite 1425
Arlington, VA 22203-1995

10. SPONSOR / MONITOR'S ACRONYM(S)

ONR

11. SPONSOR / MONITOR'S REPORT NUMBER(S)

12. DISTRIBUTION / AVAILABILITY STATEMENT

DISTRIBUTION STATEMENT A: Approved for public release; distribution is unlimited.

13. SUPPLEMENTARY NOTES

14. ABSTRACT

We report on the recent study to implement and test the schemes for calculating the skin sea surface temperature in the Navy's Coastal Ocean Model (NCOM). This includes three schemes for estimating the temperature anomaly (i.e., the correction) in the ocean cool skin, and a fourth scheme for estimating the temperature anomaly in the warm layer that may develop in the near subsurface depths due to solar heating. Coding details of the implementation are documented. Applications of the schemes are made, and the results are compared with field measurements. To understand the behaviors of the schemes, the model results from different applications are also compared with each other. Of particular note is the issue of possibly double-counting the effect of solar radiation when the warm-layer correction scheme is applied in an ocean model with sufficiently fine vertical resolution in the upper depths, since the modeled temperature field has already accounted for the solar heating. Some further improvements are discussed, including feeding the effects of skin sea surface temperature into the ocean model integration when NCOM is run stand-alone without being coupled with an atmospheric model.

15. SUBJECT TERMS

Air-sea interfacial temperature
Bulk–skin SST difference
Ocean cool skin
Warm layer

16. SECURITY CLASSIFICATION OF:			**17. LIMITATION OF ABSTRACT**	**18. NUMBER OF PAGES**	**19a. NAME OF RESPONSIBLE PERSON**
					Jie Yu
a. REPORT	**b. ABSTRACT**	**c. THIS PAGE**	U	22	**19b. TELEPHONE NUMBER** *(include area code)*
U	U	U			(288) 688-5710

This page intentionally left blank.

CONTENTS

FIGURES

COOL-SKIN AND WARM-LAYER CORRECTIONS TO SEA SURFACE TEMPERATURE IN NCOM

1. INTRODUCTION

The temperature at the air-sea interface is a key variable governing the exchange of momentum, energy and gases between the oceans and atmosphere, thus fundamentally important to the dynamical responses of both systems. It is not surprising that tremendous efforts have been devoted to accurately represent the sea surface temperature (SST) in ocean forecasting systems. SST is the most commonly observed quantity in the oceans, but also a variable that is difficult to precisely define because of the complex temperature structure in the upper ocean depths (Donlon et al., 2007). It has long been recognized that a molecular sublayer exists in the ocean at the air-sea interface, in which viscous effects dominate and heat transfer occurs by conductive diffusion. The thickness of this viscous sublayer is typically less than 1 mm. Because of surface winds, the heat flux due to molecular conductivity in the viscous sublayer is generally from ocean to atmosphere, and thus the sublayer is called the cool skin of the ocean. The temperature of the sublayer is therefore termed as the skin sea surface temperature (SSST), while the bulk SST is usually referred to the water temperature at various near-surface depths ranging from several centimeters to a few meters (Alappattu et al. 2017; Pimentel et al., 2018).

The cool skin is almost always present, and the temperature difference across the thin skin is typically 0.1 - 0.5°C (Fairall et al., 1996a), while the bulk-skin SST difference can be of O(1°C) depending on the depth of bulk SST (e.g., Alappattu et al. 2017). This is substantial, since the atmospheric response is sensitive to SST variations. For instance, to estimate the global heat balance with an uncertainty less than 10 W/m^2, the error in SST must be limited to 0.2°C (Fairall et al., 1996b). Obviously, ocean general circulation models cannot resolve the structure of the skin layer due to computational limitations. In most ocean models, SST is the temperature in the uppermost layer, thus effectively the bulk SST. In atmosphere and ocean models, bulk formulas are often used to estimate the latent and sensible heat fluxes at the air-sea boundary (Fairall et al., 1996b; Kara et al., 2000). Theoretically speaking, it is the skin SST (i.e., the temperature of water in direct contact with air) that should be used in such calculations, but models often use the bulk SST (e.g., the temperature in the uppermost layer of an ocean model).

On the other hand, various measurements are used to constrain the SST (e.g., data assimilations) in ocean models and forecasting systems. In 1972 the National Oceanic and Atmospheric Administration (NOAA) used a radiometer onboard a satellite to measure ocean surface temperature. According to the classification in Donlon et al. (2007), measurements by infrared radiometers typically represent the skin temperatures within the thermal sublayer at depths of ∼10–20 μm, while microwave radiometers measure the temperatures at depths of ∼1–1.5 mm (i.e., the subskin depths). In-situ measurements, e.g., using thermistors on submerged instruments on buoys, from ships or autonomous gliders, are bulk SST. Some satellite products are calibrated to bulk SST at designated depths, while others represent the skin or subskin SST. Clearly, applications of SST data in ocean models must recognize and reconcile the discrepancies between different sources.

Manuscript approved November 2, 2023.

In this report, we present recent work to implement and test various schemes to calculate the SSST in the Navy's Coastal Ocean Model (NCOM). NCOM is a core model component in the Navy's Coupled Ocean/Atmospheric Mesoscale Prediction System (COAMPS®[1]), as well as a stand-alone ocean model. NCOM uses an Arakawa C grid, and calculates temperature and salinity fields at cell centers. The NCOM SST thus is the temperature field at the mid-depth of the uppermost layer. For typical NCOM configurations, the resting mid-depth of the uppermost layer can be about 0.5 m. Prior to this work, this is the NCOM SST that is exported as the "sea surface temperature", or used to calculate the latent and sensible heat fluxes from the bulk formula (if such an option is selected for setting up the surface forcing; see the discussion in Section 4). In this model improvement, we implement schemes for estimating the skin-bulk temperature difference, thus obtaining the NCOM SSST. In the literature, two factors are generally acknowledged to affect the SSST: the above-mentioned cool skin and the warm layer. The latter develops due to the absorption of short-wave solar radiation in the upper ocean and lack of wind-induced turbulent mixing, and compensates the effect of skin cooling. The warm-layer thickness is typically of O(1 m). Obviously, the accuracy to resolve the structure of warm layer in an ocean model depends on the resolution of vertical grids in the upper depths.

The rest of the report is organized as follows. In Section 2, we present four schemes from the literature, and discuss their theoretical backgrounds. Three of the four schemes provide the estimate of cool-skin correction (i.e., the anomaly), and the fourth scheme calculates both the cool-skin and warm-layer corrections. In Section 3, the coding details of implementation are documented. In Section 4, we discuss the results from simulations applying the schemes, and the verification against a field dataset. Summary and future works follow in Section 5.

2. THE CORRECTION SCHEMES IN NCOM

In NCOM, the uppermost layer is always in the σ-coordinate, following the movement of sea surface. Thus, the z-elevations of grid-cell centers in the uppermost layer, at which the NCOM SST field is calculated, change dynamically and vary horizontally. When skin-cooling is the only correction to be considered, $\mathrm{SSST} = \mathrm{SST} + \Delta T_s$, where $\Delta T_s < 0$ is the temperature anomaly across the skin. When the correction due to the effect of warm layer is also considered, $\mathrm{SSST} = T_b + \Delta T_s + \Delta T_w$, where $\Delta T_w > 0$ is the anomaly across the warm layer and T_b is the bulk SST taken at a subsurface depth of O(1 m).

2.1 The original S67 scheme of skin-cooling

Making analogous to the viscous sublayer in a turbulent boundary layer, Saunders (1967; hereafter referred to as S67) proposed that the skin thickness

$$\delta \sim \nu / \sqrt{\tau_a / \rho}, \tag{1}$$

where τ_a is the wind stress at the sea surface, ρ and ν are the density and viscosity of seawater. In the molecular sublayer, heat transfer is dominated by thermal conduction, thus

$$Q \sim k \Delta T_s / \delta, \tag{2}$$

[1] COAMPS® is a registered trademark of the U.S. Naval Research Laboratory

where k is the thermal conductivity of seawater, and $Q < 0$ is the net heat flux *from ocean to atmosphere*, accounting for the sensible, latent and long-wave radiative heat fluxes. In NCOM, heat fluxes are defined to be positive downward. Introducing a proportional coefficient λ, Saunders wrote from (1) and (2),

$$\delta = \frac{\lambda \nu}{u_*}, \tag{3}$$

$$\Delta T_s = \frac{Q\delta}{k}, \tag{4}$$

where $u_* = \sqrt{\tau_a/\rho}$ is the friction velocity of seawater. Saunders suggested that the constant λ may vary from 5 to 10, and estimated $\lambda = 7$ for the observations in Hasse (1963). Clearly, as $u_* \to 0$, $\Delta T_s \to -\infty$. For low wind conditions, it is anticipated that the S67 scheme tends to overestimate the skin-cooling effect.

2.2 The modified S67m scheme of skin-cooling

Fairall et al. (1996a) and Wick et al. (1996) suggested that Q in (4) should be modified to account for the effect of short-wave radiation, which reduces the cooling rate. Given the solar radiation R_{sw}, the mean flux absorbed within the skin layer is defined as $R_{sw}f_s$, where f_s describes the absorption in different wavelength bands. As an approximation, the mean absorption is written as (Fairall et al., 1996a)

$$f_s = 0.137 + 11\delta - \frac{a}{\delta}\left(1 - \mathrm{e}^{-\delta/b}\right), \tag{5}$$

where $a = 6.6 \times 10^{-5}$ and $b = 8 \times 10^{-4}$. Thus, accounting for solar radiation, we rewrite (4) as

$$\Delta T_s = \frac{\lambda\,(Q + R_{sw}f_s)\,\nu}{k u_*}. \tag{6}$$

Fairall et al. (1996a) and Wick et al. (1996) both used a formula to calculate the Saunders constant λ, i.e.,

$$\lambda = 6\left[1 + \left(\frac{16 Q_b g \alpha \rho c_p \nu^3}{u_*^4 k^2}\right)^{3/4}\right]^{-1/3}, \tag{7}$$

where g is the gravitational acceleration, α and c_p are, respectively, the coefficient of thermal expansion and specific heat of seawater. The virtual surface heat flux Q_b accounts for the buoyancy effect of salinity due to evaporation and is given by

$$Q_b = Q + \left(\frac{S\beta c_p}{\alpha L_e}\right) Q_e, \tag{8}$$

where S is the mean salinity, β is the salinity expansion coefficient, L_e is the latent heat of vaporization of seawater, and Q_e is the latent heat flux. For wind speeds above approximately 3 m/s, $\lambda \to 6$ (Wick et al. 1996). Formula (6), together with (7) and (8), is referred to as the modified Saunders scheme, S67m.

2.3 The SS94 scheme of skin-cooling based on surface renewal

Another treatment of the molecular sublayer at air-sea interface is the surface renewal approach. It assumes that the surface sublayer undergoes a cyclic process of growth and destruction based on the theory of free convection at high Rayleigh numbers (Howard, 1964): The boundary layer forms by thermal diffusion and grows in thickness until convective instability develops. This induces turbulent mixing, leading to bursts of ejection/injection of fluid elements into/from the bulk fluid, thus destroying the laminar sublayer. Assuming that the local bursts of destruction occur randomly (i.e., the probability for a fluid element to break away from the sublayer is independent of the time that the element has resided at the surface), Liu and Businger (1975) derived a horizontally averaged temperature profile in the sublayer. Following Liu and Businger, Soloviev and Schlüssel (1994; hereafter referred to as SS94) proposed a parametrization of skin-cooling ΔT_s based on surface renewal, i.e.,

$$\Delta T_s = (q/u_*)\,\Lambda_0 \mathsf{Pr}^{1/2}\,(1+\mathsf{Rf}_0/\mathsf{Rf}_{cr})^{-1/4}\,(1+\mathsf{Ke}/\mathsf{Ke}_{cr})^{1/2}, \tag{9}$$

where the ocean cooling/heating rate $q = Q/\rho c_p$, the Prandtl number $\mathsf{Pr} = \nu/\mathscr{D}$ with $\mathscr{D}$ being the thermal diffusivity of seawater, the Keulegan number $\mathsf{Ke} = u_*^3/g\nu$, and the surface Richardson number $\mathsf{Rf}_0 = -\alpha g q \nu u_*^{-4}$. Recall that $q<0$ for ocean surface cooling. Based on the data in Grassl (1976), SS94 suggested $\Lambda_0 = 13.3$, and the critical values $\mathsf{Ke}_{cr} = 0.18$, $\mathsf{Rf}_{cr} = 1.5\times10^{-4}$. Note that in (9) q includes the sensible, latent and long-wave radiative heat fluxes, but does not include the solar radiation. It should also be mentioned that in their original formulation SS94 defined $q>0$, hence had negative values for Rf_0 and Rf_{cr}. SS94 stated that (9) works for a wide range of wind conditions; for moderate wind speed conditions it is similar to S67, while for calm weather conditions it asymptotically agrees with Katsaros et al. (1977).

2.4 The ZB05 scheme for warm-layer anomaly

Fairall et al. (1996a) addressed the effect of warm layer, pointing out that daytime solar heat into the ocean is mostly absorbed in the upper few meters, hence can result in a stably stratified surface layer in the absence of wind-induced turbulent mixing, and the warming effect may even persist well past sundown. To account for this effect, they suggested that SSST = $T(z_d)+\Delta T_s+\Delta T_w$, where $T(z_d)$ is the subsurface temperature at a reference depth $z_d=-d$ (for instance, the depth of temperature measurements), $\Delta T_s<0$ is the skin-cooling anomaly as discussed above, and $\Delta T_w>0$ is the wave-layer anomaly. While Fairall et al. (1996a) gave a parametrization for ΔT_w, Zeng and Beljaars (2005; hereafter referred to as ZB05) proposed that ΔT_w evolves in time according to

$$\frac{\partial \Delta T_w}{\partial t} = \frac{Q+R_{sw}-R(-d)}{d\rho c_p \gamma/(\gamma+1)} - \frac{(\gamma+1)\kappa u_*}{d\phi_t(d/L)}\Delta T_w, \tag{10}$$

where $\kappa=0.4$ is the von Kármán constant, γ is an empirical parameter,

$$\frac{R(-d)}{R_{sw}} = 0.28\mathrm{e}^{-71.5d} + 0.27\mathrm{e}^{-2.8d} + 0.45\mathrm{e}^{-0.07d} \tag{11}$$

is the normalized solar radiation flux at $z_d=-d$ following Paulson and Simpson (1981), and

$$\phi_t(d/L) = \begin{cases} 1+5d/L & \text{for } d/L\ge 0 \\ (1-16d/L)^{-1/2} & \text{for } d/L<0 \end{cases} \tag{12}$$

is the stability function with the Monin-Obukhov length

$$L = \rho c_p u_*^3 / \left[\kappa g \alpha (Q + R_{sw} - R(-d))\right]. \tag{13}$$

ZB05 suggested that the warm-layer depth $d = 2 \sim 4$ m may be appropriate where the diurnal fluctuation of ocean temperature is minimal. For $d = 3$ m, ZB05 suggested that $\gamma = 0.3$. For ΔT_s, ZB05 used the same calculation as in S67m. (Note that equation (6) in ZB05 is incorrect. To calculate the skin thickness δ, we use (3) with (7) as given above.)

3. CODE IMPLEMENTATION

A new subroutine *oskinsst* is added to the NCOM source code, which contains the calculations of ΔT_s and ΔT_w using the schemes discussed in Chapter 2. A call to *oskinsst* is made in subroutine *omodel* whose task is to advance the ocean model fields on each grid/nest, including the time integration and grid-grid interactions. Coding details are documented, as follows.

(I) On calculating λ using (7). For seawater in the oceans, $S\beta \simeq 0.026$ and relatively invariant, and the coefficient of thermal expansion $\alpha \simeq 3 \times 10^{-4}\mathrm{K}^{-1}$ in tropics and decreases to $\sim 10^{-5}\mathrm{K}^{-1}$ in polar and cold regions. For typical ocean surface conditions, the buoyancy effect of salinity due to evaporation (i.e., the second term on the right hand of (8) for the virtual surface heat flux Q_b) is relatively small. For instance, Fairall et al. (1996a) estimated that Q_b differs from Q by less than 10% for the light wind conditions (< 4.0 m/s) during the Tropical Ocean-Global Atmosphere (TOGA) Coupled Ocean-Atmosphere Response Experiments (COARE) in 1992-1993 (Webster and Lukas, 1992). In NCOM, the latent heat flux Q_e is included in the net surface heat flux (variable *rsflx*) and not separately stored. To calculate the buoyancy effect of salinity due to evaporation, additional code modifications are needed to either retain Q_e from the input data files or calculate it within subroutine *oskinsst* during the run time. In view of its relatively minor influence, as discussed in Fairall et al. (1996a), in this development we take $Q_b = Q$ in (7) when calculating the Saunders constant λ.

(II) On time-stepping the warm-layer equation (10). The numerical integration is carried out using a semi-implicit Euler method. Denoting time steps using the superscripts, the finite-difference representation of (10) is written as

$$\frac{\Delta T_w^{n+1} - \Delta T_w^n}{\Delta t} = \left[\frac{Q + R_{sw} - R(-d)}{d\rho c_p \gamma/(\gamma+1)}\right]^n - \left[\frac{(\gamma+1)\kappa u_*}{d\phi_t(d/L)}\right]^n \Delta T_w^{n+1}, \tag{14}$$

which leads to

$$\Delta T_w^{n+1} = \left\{\Delta T_w^n + \Delta t \left[\frac{Q + R_{sw} - R(-d)}{d\rho c_p \gamma/(\gamma+1)}\right]^n\right\} \left\{1 + \Delta t \left[\frac{(\gamma+1)\kappa u_*}{d\phi_t(d/L)}\right]^n\right\}^{-1}. \tag{15}$$

(III) In NCOM, surface heat and radiative fluxes are converted into the ocean heating/cooling rates $q = Q/\rho c_p$. When implementing the cool-skin and warm-layer corrections, all formulas are rewritten using

q and the thermal diffusivity $\mathscr{D}$ (instead of the thermal conductivity k) so that the factor ρc_p cancels out. Recall that $\mathscr{D} = k/\rho c_p$.

(IV) Three new ocean model fields are declared on each grid/nest: *ssst* for the skin sea surface temperature, *dtskin* for the skin-cooling anomaly ΔT_s, and *dtwm* for the warm-layer anomaly ΔT_w. Correspondingly, three new pointer variables, *possst, podtskin, podtwm*, are declared. The module *NCOM_Init* sets pointers and allocates memory for ocean model fields on each grid, which is modified accordingly. At each time step on each grid, the anomalies are added onto the appropriate temperature field (i.e., the temperatures in the uppermost layer if S67, S67m, or SS94 is used, or the temperatures interpolated at z_d if ZB05 is used), and the resultant values are assigned to *ssst*. The NCOM SST field remains unaffected, i.e., the corrections are not fed into the model integration when NCOM is run without being coupled to the atmospheric model.

(V) When two-way grid nesting is enabled, the feedback from child grids (i.e., the fine-mesh nests) to their parent grid is first performed. That is, SSST is calculated using the parent grid T field that has been updated by the fine-mesh results from the nests.

(VI) Subroutine *write_ff* outputs the flat-files of ocean fields at specified time intervals. This is modified to output *ssst, dtskin, dtwm*. A user specifies the output frequencies for individual model fields using the namelist *omnloff*, whose variables are declared in *COMMON.h*. Codes are updated accordingly to accommodate the new variables.

(VII) The namelist *parmlst*, which contains a list of user-specified parameters for model configuration, is modified to include the selection of ocean skin SST options and inputs of physical parameters needed in the calculations; see Fig. 1. An integer variable *indssst* flags the selected scheme. The value *indssst* $= 0$ indicates that skin SST is not calculated, and is set as the default. When the ZB05 scheme is flagged, a user can specify the warm-layer depth using the designated parameter. The default values of these parameters are set in subroutine *define*. For these additions in *parmlst*, the following code modifications are made: (a) Subroutine *paramset* puts parameters in common blocks for the current grid (or gets parameters from the blocks). Codes are added for the skin SST related parameters. (b) In *COMMON.h*, new variables *iskno* and *skno* are declared to hold the skin SST related parameters in *parmlst*, and added to the appropriate blocks. (c) In *NCOMPAR.h*, the skin SST related parameters in *parmlst* are declared and added to the appropriate blocks. (d) In subroutine *write_ff*, the variable *indssst* is used to mask *offssst, offdtskin, offdtwm*. There would be no flat-file outputs of skin SST related variables when *indsst* $= 0$, and ΔT_w is only output when ZB05 is selected.

```
!  ocean skin SST options and physical parameters (iskno, skno):
indssst=  2     ,!skinSST scheme: =0 no, =1 revised Saunders(1967),=2 Zeng&Baljaars(2005),=3 Soloviev&Schlussel(1994)
znu =1.138e-6   ,!viscosity (m2/s);(1.004,1.138,1.304,1.514,1.787)e-6 at (20,15,10,5,0)degC
zkappa= 1.4e-7  ,!thermal diffusivity (m2/s);(1.42,1.40,1.38, ,1.33)e-7 at (20,15,10, ,0)degC
tcndct= 5.9e-1  ,!thermal conductivity (J/m/s/degC);(5.9,5.9,5.8,,5.6)e-1 at (20,15,10, ,0)degC
zLe = 2.4535e+6 ,!latent heat of vaporization of seawater (joules/kg)
wmdpth= 3.0     ,!the bottom of the warm layer z=-wmdpth(m)
```

Fig. 1—A segment of code (screen-shot) from the user input file for the namelist *parmlst*, showing the selection of skin SST options and relevant physical parameters.

4. VALIDATION AGAINST THE CASPER-EAST DATA

To test the implementation, we set up NCOM simulations for the US East coastal region, where the Coupled Air-Sea Processes and Electromagnetic Ducting Research East campaign (CASPER-East) was

conducted at Duck, North Carolina from 10 October to 06 November 2015; see Fig. 2. The model domain includes the Chesapeake Bay and 24 rivers. The horizontal grid dimensions are 400×400, so that the mean mesh sizes are 2.1649 km and 1.7285 km in the zonal and meridional directions, respectively. We use a total of 51 vertical layers, of which the top 35 layers are in the σ coordinate. The vertical girds are logarithmically stretched and the resting thickness of the uppermost layer is 0.5 m. For vertical mixing, the Mellor-Yamada Level 2.5 scheme (Mellor and Yamada 1982; Mellor 1996) is used. In this application, the horizontal mixing is turned off (except for the numerical dissipation associated with the 3rd order upwind schemes). The coefficient of bottom friction is calculated at each time step using the dynamic depth accounting for the movement of surface elevation. Wetting/drying is allowed. The simulation period is from 01 September to 06 November, 2015, and the time step is 45 s. The model fields are output every 3 hours.

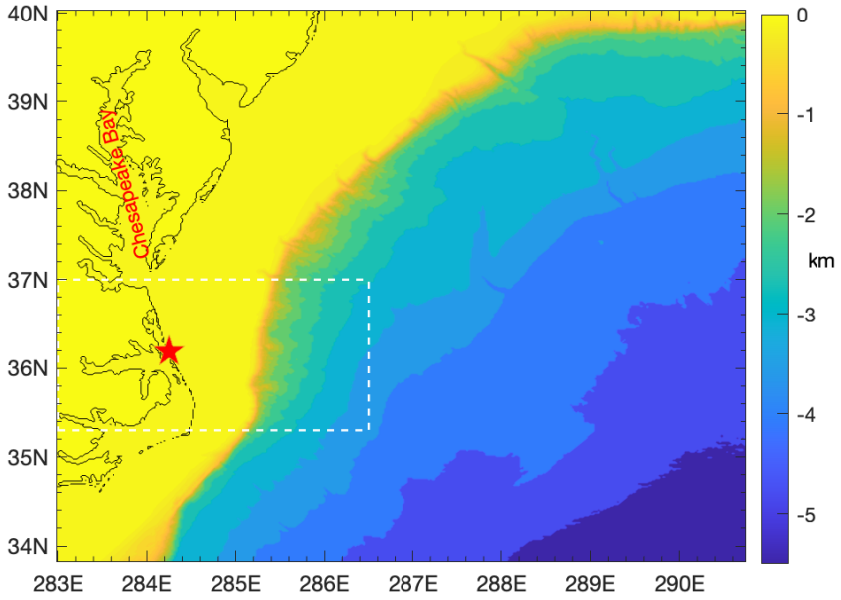

Fig. 2—Model domain showing the bathymetry (i.e., the water depths). The dashed box encloses the ship tracks during the CASPER-East campaign. The star marks the U.S. Army Corps of Engineers Field Research Facility in Duck, NC.

Input data files of surface atmospheric forcing are set up using the archived COAMPS database. The 1-hourly COAMPS fields are at 0.15° resolution. The setup was for $indsft = indsfs = 5$. With this option, NCOM reads in the long-wave heat flux from the data files during the run time, but computes the latent and sensible heat fluxes from a bulk formula (Kara et al., 2000) using modeled NCOM SST and surface atmospheric variables (air temperature, winds and humidity) from the input files. The sum of these fluxes is the net surface heat flux. With $indsfs = 5$, NCOM reads in the surface salt flux due to precipitation, but computes the surface salt flux due to evaporation from a bulk formula (Kara et al., 2000) using the computed latent heat flux just mentioned above. For stand-alone NCOM simulations, and in the absence of any constraint on the NCOM SST using observations (e.g., data assimilation), this way of setting up surface forcing is an indirect relaxation of NCOM SST to what would have been used in the atmospheric model if a coupled simulation were run.

Input data files of boundary forcing are set up by interpolating HYCOM fields from the Global Ocean Forecast System 3.1, a $1^\circ/12$ product with 3-hourly fields (Metzger et al. 2017). Tides are specified using the

Oregon State University US East Coast database (Egbert et al. 1994; Egbert and Erofeeva 2002). Monthly climatological river fluxes and temperatures from the Navy's Global River Database (Barron and Smedstad 2002) are interpolated to the nearest computational points on the model grid.

The treatments of lateral open boundary conditions (OBCs) are, (i) the Flather radiation condition for surface elevation, (ii) the Orlanski radiation condition for temperature and salinity, tangential depth-integrated transport, as well as tangential 3D velocity, and (iii) the advection condition (i.e., the internally calculated value plus upstream advection) for normal 3D velocity.

For the solar extinction profile, the 2-band exponential approximation to Jerlov types is used (Jerlov, 1976). The seawater optical type IB ($indtype = 3$) is specified in the entire model domain. The solar extinction profile is calculated at each time step on each grid to account for the change in elevations of the σ-layers due to the movement of free surface.

The CASPER-East data are shipboard measurements taken from the R/V Hugh R. Sharp during its campaign transit. The measurements include meteorological fields from the ship mast (air pressure, air temperature, relative humidity, horizontal wind speed and direction), bulk SST, and skin SST. Seawater intake for the bulk SST was located 1 m below the ship mean water line. The skin SST measurements were collected using an infrared SST autonomous radiometer (ISAR) with the reported accuracy of 0.1 K (Alappattu et al. 2017). Skin SST measurements were not taken during rain or sea-spray conditions, since the ISAR platform included a shutter to protect the optical components in such conditions. Post-processing by the CASPER-East investigators yielded a dataset that has a nominal 3 min time resolution and consists of 5034 skin SST measurements over the 27-day period. More details about the field experiment and data can be found in Alappattu et al. (2017) and Wang et al. (2018).

The model results are compared with the CASPER-East skin SST data in Fig. 3. In this study, we exclude those times when the ship was in or adjacent to port, due to anomalous values found which are likely associated with contamination by land or nearby obstructions. Those periods excluded are mostly times when the ship was at Naval Station Norfolk, which is a port with intricate coastal geography and channels that cannot be sufficiently resolved by NCOM. This exclusion amounts to the removal of approximately 41.5 hours of observations from four periods, including a 27-hour period during 10 to 11 October 2015. Since the model results are output ever 3 hours, much less frequent than the collections of data, we first locate the signal times closest to the model output times, then linearly interpolate the NCOM fields to each of those signal times identified. We then perform a bilinear spatial interpolation of the NCOM fields to the positions of data at those times.

Over 24 days, the results of NCOM SSST from all four schemes show good agreements with the ISAR data, except for two short periods around 23–25 October and 31 October–02 November; see Fig. 3a. On the other hand, the NCOM SST (which are the temperatures in the uppermost layer and same in all cases) consistently overestimate the observed skin SST, except for those two periods just mentioned; see Fig. 3b. The discrepancies in the model-data comparison are mainly caused by the NCOM SST; specifically, around 23–25 October the NCOM SST are lower than the observed sea surface temperatures by about 2.5°C. As seen in Figs. 3c, 3d, the ship track was approximately along 36.2°N latitude but zigzagged around 285.2°E (74.8°W) longitude from 23 to 25 October, and wandered in an area around 36°N 285.6°E (74.4°W) from 30 October to 02 November. The ship cruised right at the western boundary of Gulf Stream during these times; see Fig. 4. The rapid variations in the ISAR skin SST during these times are due to measurements being made crossing the Gulf Stream boundary (Alappattu et al., 2017). Since the accuracy of predicting sharp

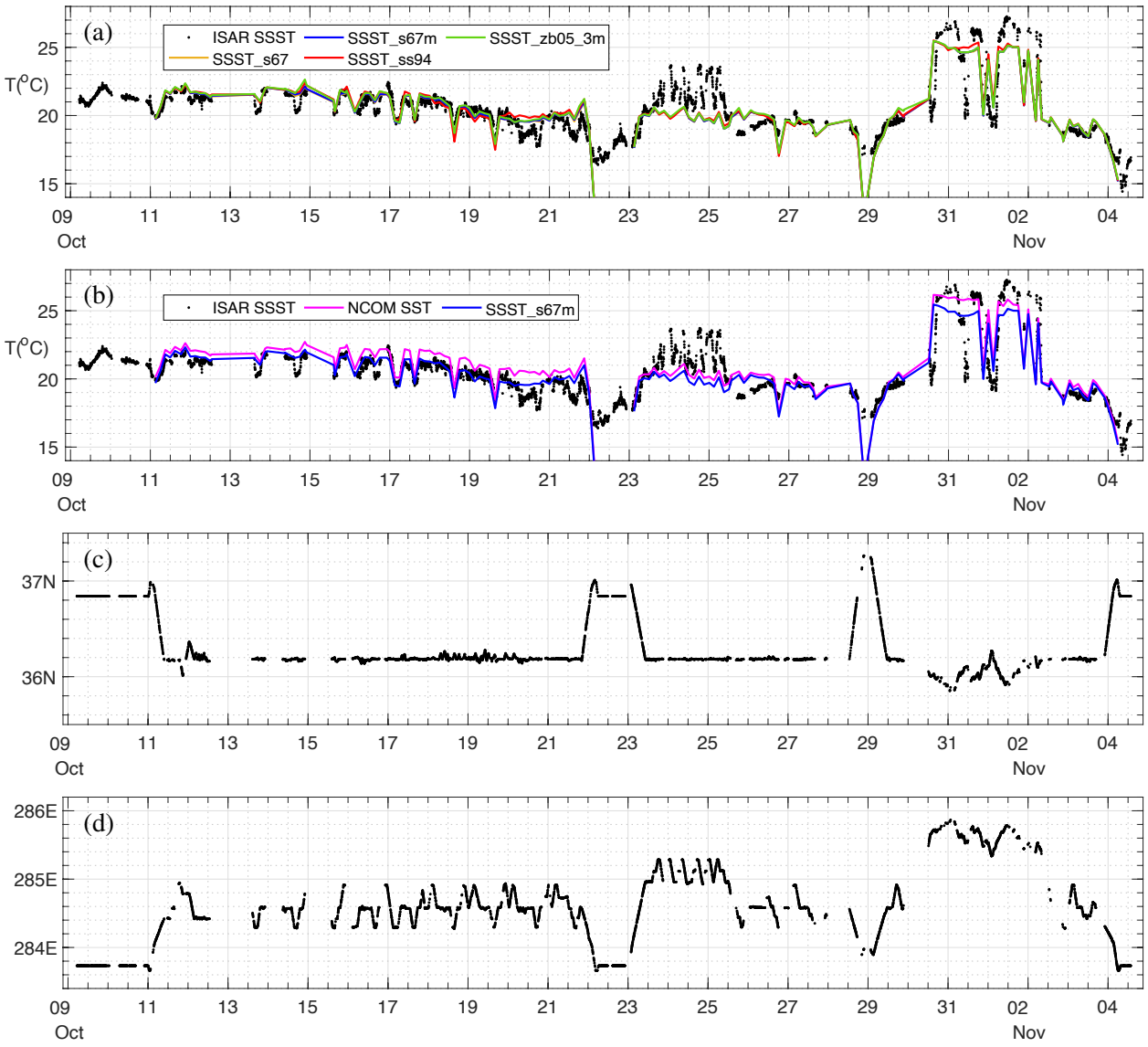

Fig. 3—CASPER-East ISAR skin SST measurements compared with (a) the NCOM SSST using the correction schemes described in Section 2, and (b) the NCOM SST (with the NCOM SSST from S67m included to illustrate the differences). The result for ZB05 is for $z_d = -3$ m, i.e., the warm-layer depth of 3 m. (c)–(d) The latitudes and longitudes of the data points.

fronts and small-scale eddies is most sensitive to grid resolution, in contrast to the prediction of large-scale flow structures, one may argue that a slight mis-match in the details of the Gulf Stream boundary can result in relatively large disagreements between the NCOM SST and ship observations (such as seen from 23 to 25 October), leading to apparently unsatisfactory comparison of SSST.

While they are nearly indistinguishable in Fig. 3a, the differences between the schemes can be seen in the skin-bulk SST difference $\Delta T = \text{NCOM SSST} - \text{NCOM SST}$, as plotted in Fig. 5. For S67, S67m and SS94, this is the skin-cooling anomaly, i.e., $\Delta T = \Delta T_s$, but for ZB05, $\Delta T = T(z_d) - \text{SST} + \Delta T_s + \Delta T_w$. Recall that the resting depth of the uppermost layer is 0.5 m in this application. Overall, ΔT from SS94 based

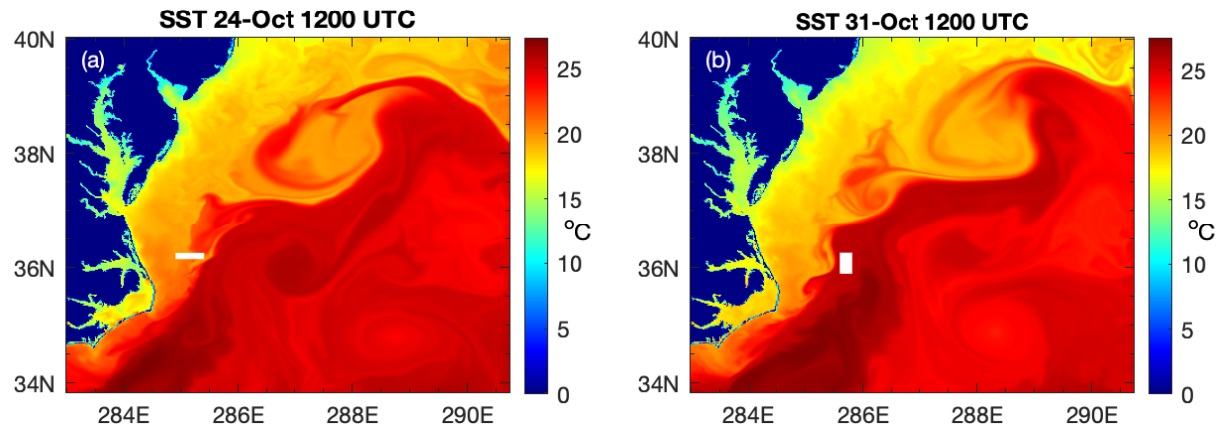

Fig. 4—NCOM SST showing the western boundary of Gulf Stream, (a) on 24 October 2015, and (b) on 31 October 2015. The white line segment in (a) and small white box in (b) indicate the ship positions from 23 to 25 October and from 30 October to 02 November, respectively.

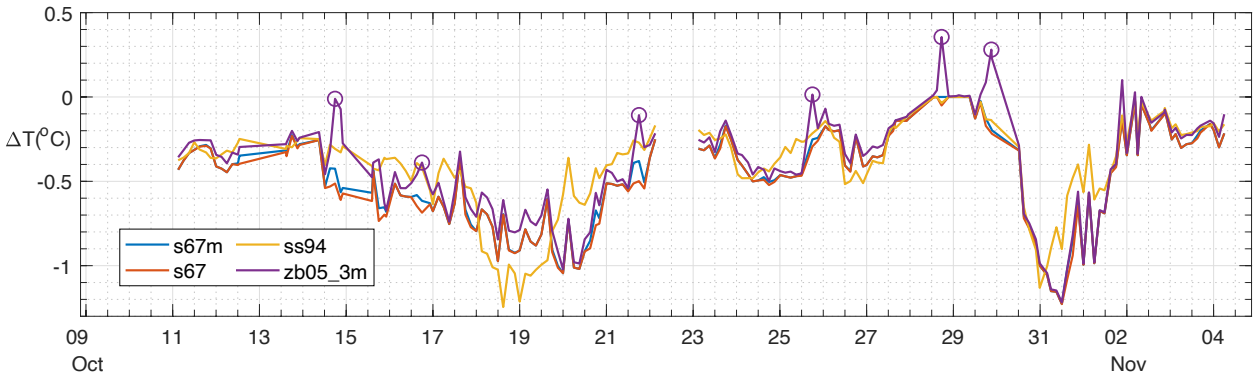

Fig. 5—Temperature anomaly $\Delta T = \mathrm{SSST} - \mathrm{SST}$ given by the NCOM simulations using the correction schemes S67m, S67, SS94, and ZB05 with $z_d = -3$ m. The open circles mark the events of largest warm-layer corrections (see Table 1).

on surface renewal shows a greater difference from that given by other schemes. Since short-wave solar radiation $R_{sw} f_s$ compensates skin cooling Q, the anomaly ΔT given by S67m in (6) is smaller in magnitude than that from S67 in (4) when the solar heat flux is strong. Recall that the effect of warm layer originates from solar heating. Thus, when there is a large difference between ΔT given by S67m and S67, it indicates a strong warm-layer effect. In Fig. 5, the events of largest warm-layer anomalies are marked. They are seen to be correlated with noticeable difference between ΔT given by S67m and S67. Eastern Daylight Time (EDT) represents the local time, and is 4 h behind the Coordinated Universal Time (UTC). As seen in Table 1, most of these events occurred in early afternoons, slightly after the peak of daytime solar heating. On 29 October, however, a large warm-layer correction occurred at 17:01 EDT, while there is little difference in the values of ΔT given by S67m and S67 because of the diminishing solar heating close to sundown. The time-delayed, nonlocal effect is typically captured by a differential equation, such as the evolution equation (10) for ΔT_w, but not easily described by parameterization. This delayed effect of warm layer is consistent with the remarks by Fairall et al. (1996a) that measurable warming effects in the upper 20 m may persist well past sundown. However, the large magnitudes of ΔT_w are open for debate (see the discussion below).

Table 1—Points marked in Fig. 5, showing the strongest effect of warm layer from the simulation using ZB05 with $z_d = -3$ m.

ΔT (°C)	-0.0109	-0.3888	-0.1076	0.0144	0.3554	0.2807
UTC	14/10 17:50	16/10 17:57	21/10 18:01	25/10 18:00	28/10 17:28	29/10 21:01
EDT	14/10 13:50	16/10 13:57	21/10 14:01	25/10 14:00	28/10 13:28	29/10 17:01

The temperature anomaly field, $\Delta T = \mathrm{SSST} - \mathrm{SST}$, is shown at various times on 21 October in Fig. 6 for the results using the S67, S67m, and SS94 schemes (which only apply the skin-cooling correction), and in Fig. 7 for the results using ZB05 with different values of z_d for the warm-layer depth. The same color scale is used in both figures for easy comparison, even though ΔT is non-positive in Fig. 6. The UTC times selected represent the local hours at night, morning, and late afternoon. At nighttime, there is virtually no difference between the results from S67 and S67m, as expected. With the solar heating during daytime hours, S67m tends to give slightly smaller (in magnitude) skin-cooling corrections than S67 does in the shallow waters near the coast and in the estuary and rivers, as well as inside the Gulf Stream. This is particularly noticeable as the solar heating peaks (cf. Figs. 6b and 6e). In comparison, the surface renewal model SS94 gives much weaker skin-cooling corrections, in particular inside the Gulf Stream.

With the effect of warm layer, the results from ZB05 with $z_d = -5, -3$ m are seen to be similarity to that from S67m at the nighttime and morning hours, though differences are noted in the shallow coastal waters; near the sunset hours, the differences intensify and spread into the Gulf Stream (cf. Figs. 7a–7c, Figs. 7d–7f with Figs. 6d–6f). When we change the warm-layer depth, the result with $z_d = -5$ m is fairly close to that with $z_d = -3$ m. The differences between the two are mostly in the shallower coastal areas, and at sunset hours. This seems to indicate that the diurnal fluctuation of seawater temperature is minimal in the depth-range of 3 to 5 m in the region. In contrast, the result with $z_d = -1$ m shows patches of very warm surface waters, particularly at sunset hours, which seem to be abnormal (see Fig. 7i).

The time series of ΔT and surface friction velocity of sea water u_* at a grid point 36.2052°N 284.7916°E (75.2084°W) near the ship tracks are plotted in Fig. 8 over the 7-day period from 16-22 October 2015. A few remarks are worth making.

(i) *On the diurnal fluctuation of bulk-skin SST difference*: The diurnal signature is clearly seen in the variability of ΔT with local time from the results given by S67m, S67, and ZB05 with $z_d = -3$ m, but is weak in the result given by SS94. Alappattu et al. (2017) observed that under low wind conditions larger values of bulk-skin SST difference (i.e., $-\Delta T$) tend to occur before sunrise and after ∼1500 EDT. Such a pattern of diurnal fluctuation with dual maximum of ΔT is variably predicted by S67m, S67, and ZB05 with $z_d = -3$ m. For instance, it is seen in the results from all three schemes on 17 Oct when the daytime wind condition is low, and even on 18 Oct when the wind condition is relatively high, but not seen under the similarly low wind conditions on 16 and 20 Oct. Furthermore, S67m predicts two local maxima of $-\Delta T$, one before 0900 EDT and one after 1500 EDT, on both 21 and 22 Oct when the wind conditions are fairly low, while S67 predicts little variation in ΔT before 1800 EDT on 21 Oct, and ZB05 predicts much warmer SSST from afternoon to sunset on both days.

(ii) *On the surface renewal model SS94*: The variability of ΔT given by SS94 shows a different pattern from that given by S67m, S67, or ZB05. It is especially interesting to note that when the wind condition

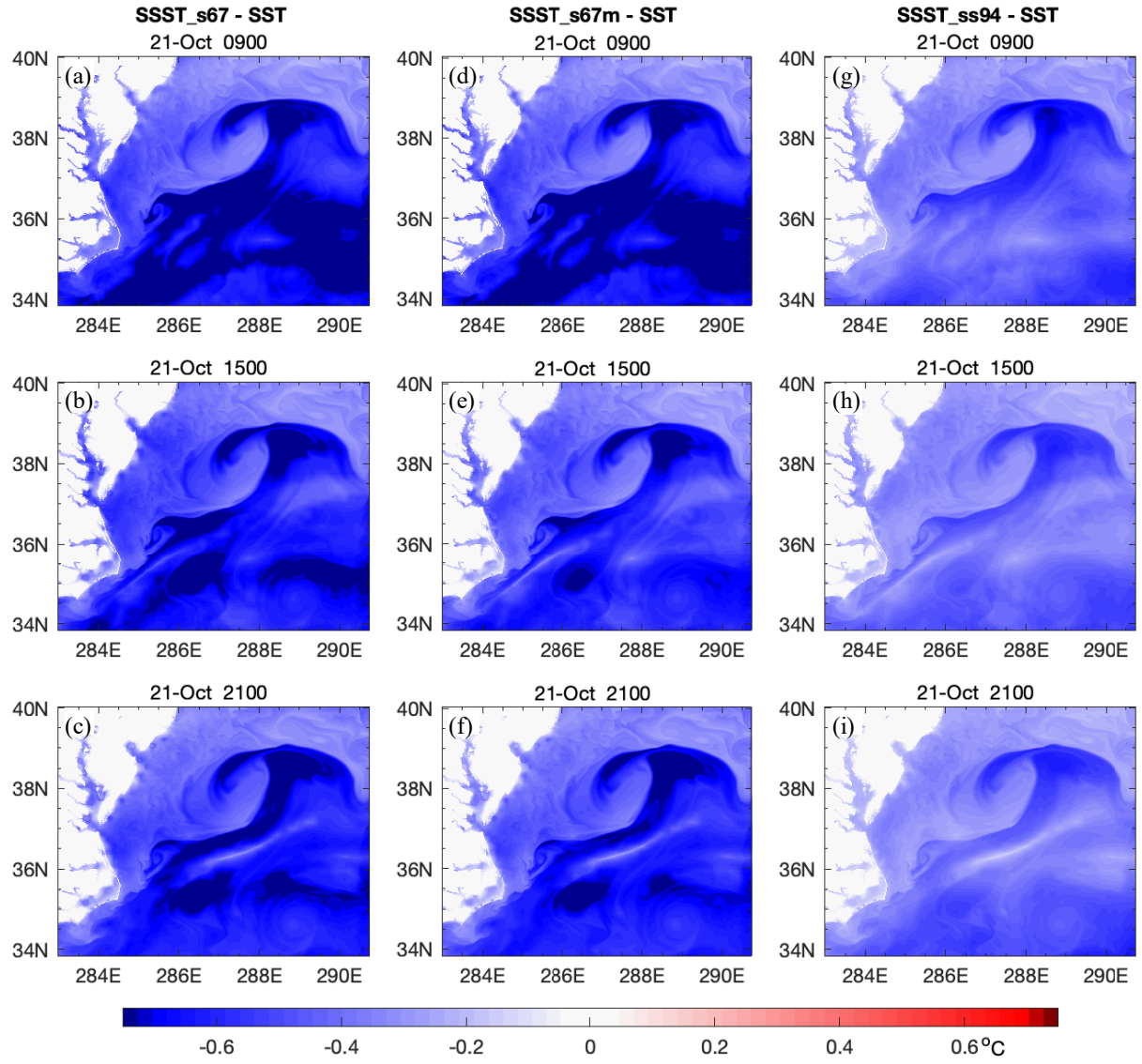

Fig. 6—Temperature anomaly field ΔT at various times on 21-Oct-2015, from NCOM simulations using the correction schemes S67, S67m, SS94. The UTC times are shown. The local time (EDT) is 4 h behind.

rapidly changes, the direction of changing ΔT (i.e., the gradient $\mathrm{d}\Delta T/\mathrm{d}t$) predicted by SS94 tends to be opposite from that given by other schemes; for example, see the events on 15-Oct 0300 EDT and 1500-2100 EDT, 17-Oct 0300-0900 EDT and 2100 EDT, 18-Oct 1800 EDT, and 19-Oct 0900-1800 EDT. This may be related to the critical values of surface Richardson number Rf_{cr} and Keulegan number Ke_{cr}, which are hardwired in the code in the present development. More comprehensive analysis of ocean surface conditions is needed to understand the model behaviors.

(iii) *On the warm-layer correction*: The ZB05 scheme with $z_d = -3$ m generally underestimates the bulk-skin SST difference $-\Delta T$, when compared with S67m and S67, but three schemes nevertheless give strikingly similar variability of ΔT with local time. The underestimation is mostly about 0.1°C or less,

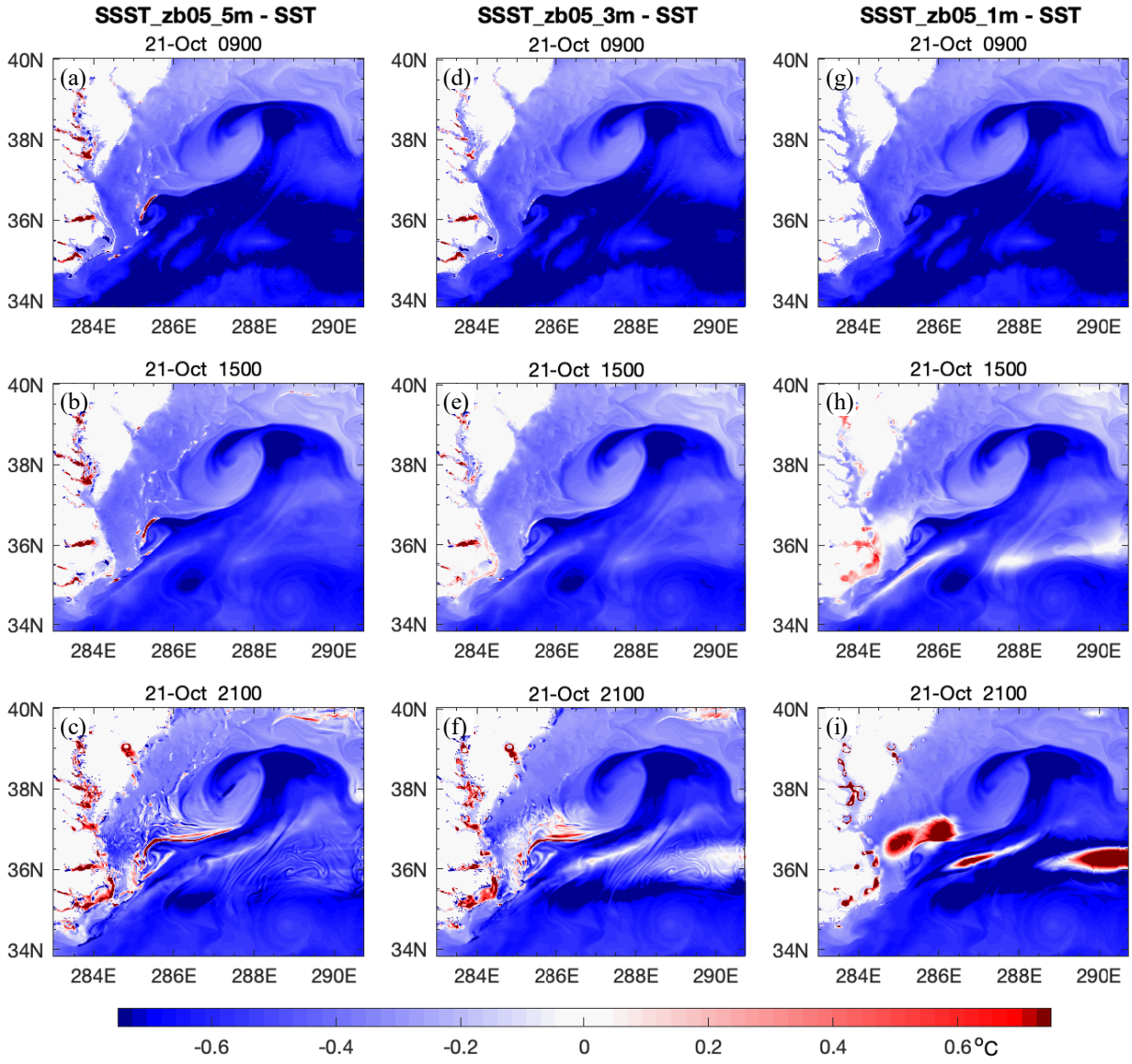

Fig. 7—Temperature anomaly field ΔT at various times on 21-Oct-2015, from NCOM simulations using ZB05 with $z_d = -5, -3, -1$ m, respectively. The UTC times are shown.

but large warm-layer corrections are noticed on 21-22 Oct. Recall that $\Delta T = \Delta T_s$ for S67 and S67m, while $\Delta T = T(z_d) - \mathrm{SST} + \Delta T_s + \Delta T_w$ for ZB05. This means that $T(z_d) - \mathrm{SST}$ approximately cancels ΔT_w (with a residual of $\sim 0.1^\circ$C), except for the above-mentioned two days with events of large ΔT_w. This indicates that the NCOM temperature field in the near surface depths represents the development of warm layer due to short-wave solar radiation. Indeed, the logarithmically stretched NCOM vertical grids have a resolution that there are 5 layers above the resting depth $z = -3.50$ m, and the solar extinction profile specified is of Jerlov types. Denoting $\widetilde{\Delta T}_w = \mathrm{SST} - T(z_d)$, this quantity represents the warm-layer anomaly that is given by the NCOM prediction of temperature distribution, and is of $\sim 0.1^\circ$C less than ΔT_w estimated by ZB05 with $z_d = -3$ m (excluding the comparison on 21-22 Oct), in view of the above discussion. Note that the warm-layer equation (10) from ZB05 does not describe the

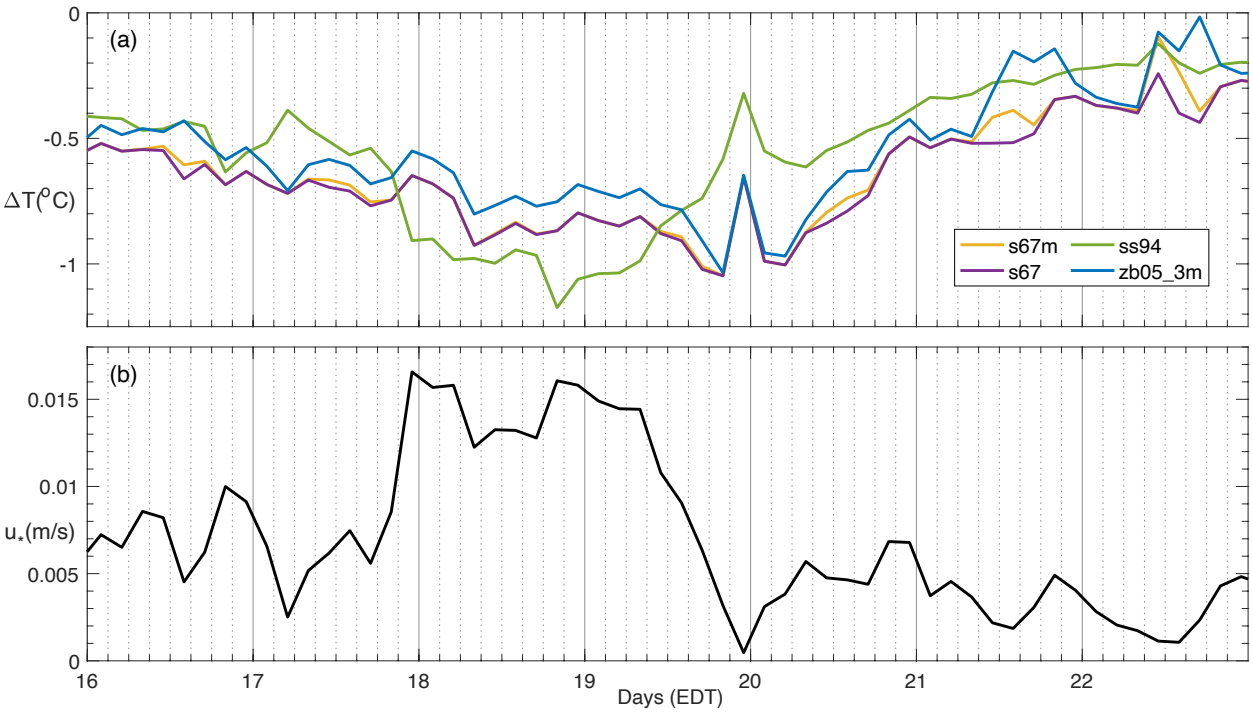

Fig. 8—Time series of temperature anomaly ΔT in (a) and surface friction velocity of seawater u_* in (b) at 36.2052°N 284.7916°E on 16-22 October 2015. The local hours (EDT) of the day are given by the minor ticks with a 3-hour interval.

actual temperature distribution across the layer but only estimates the temperature difference between the top and base of the layer. Thus, unless the warm-layer depth z_d is carefully chosen there is a risk of "double counting" the effect of solar radiation when using ZB05 to calculate the SSST from the NCOM temperature field of a sufficiently fine vertical resolution. This can be seen in Fig. 9 where the time series of ΔT from ZB05 with $z_d = -5, -3, -1$ m are compared. It is especially interesting to notice the warm-layer corrections on 21-22 Oct. Although thicker warm layers and stronger effects are expected on these two days (indicated by the fairly low wind conditions; see Fig. 8b), the increasingly large magnitudes of ΔT_w with shallower depths z_d are highly questionable, and likely due to double counting the effect of solar radiation. With $z_d = -5$ m, the result given by ZB05 is better compared with that by S67m.

5. SUMMARY AND FUTURE DEVELOPMENT

We have given the details of implementing various schemes to compute the skin sea surface temperatures SSST in NCOM, and verification against field observations. Three options are provided for calculating the skin-cooling correction: (i) the S67 scheme from Saunders (1967), (ii) the modified Saunders scheme S67m as proposed in Fairall et al. (1996a) to include the short-wave solar heating hence reduces the skin cooling flux, and (iii) the SS94 scheme from Soloviev and Schlüssel (1994) based on modeling surface renewal. The fourth option is the ZB05 scheme from Zeng and Beljaars (2005) which applies both skin-cooling and warm-layer corrections. For S67, S67m, and SS94, the SSST field is calculated by adding the skin-cooling anomaly to the NCOM SST in the uppermost layer. The ZB05 scheme calculates the SSST field by adding

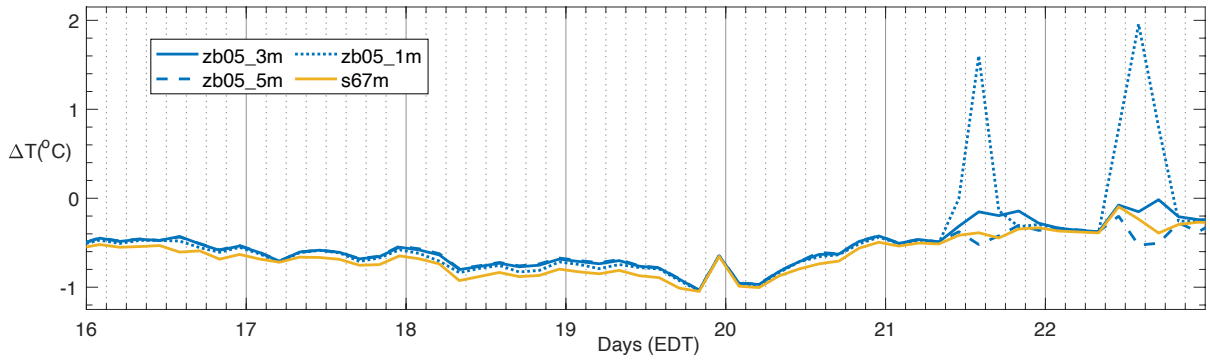

Fig. 9—Comparison of the time series of ΔT given by ZB05 with different z_d at 36.2052°N 284.7916°E on 16-22 October 2015. The result given by S67m is included as a reference. The local hours (EDT) of the day are given by the minor ticks with a 3-hour interval.

the skin-cooling and warm-layer anomalies to the bulk temperature at a specified subsurface depth (i.e., the warm-layer depth).

The implementation is tested against the skin SST measurements over a 24-day period from the CASPER-East experiment. Good agreements with the data are found from the NCOM SSST given by all four schemes, while the conventional NCOM SST mostly overestimate the data. This indicates that the implemented SSST schemes perform as expected. The large discrepancies during two short periods from 23–25 October and from 31 October to 02 November 2015 are due to the fact that the measurements at those times are highly variable as they were made crossing the western boundary of the Gulf Stream. Since the accuracy of predicting sharp fronts and small-scale eddies is very sensitive to grid resolution, the unsatisfactory model-data comparison during these times does not suggest the inadequacy of SSST schemes, but rather an issue of ocean model fidelity. An improved comparison can be expected when a higher resolution ocean model is used to more accurately capture the structure and movement of the boundary of the Gulf Stream, and/or data assimilation is included to constrain the model SST.

While all schemes performed similarly when compared with the CASPER-East data, a few points are worth emphasizing, which suggest future works.

(a) The differences between the S67 and S67m scheme become greater as daytime solar heating peaks. This is expected. The differences are particularly noticeable near the coastline, and in the estuary and rivers, but also occur in areas offshore inside the Gulf Stream. The differences are expected to be correlated with the absorption of short-wave solar radiation. In this development, we use the mean absorption in Fairall et al. (1996) which essentially follows Paulson and Simpson (1981) and does not reflect the variability of solar attenuation in waters of different optical types. There are suggestions to adjust the absorption coefficients associated with shorter wavelengths based on Jerlov water types (e.g., Soloviev and Schlüssel, 1996; Verevochkin and Startsev, 2005; Pimentel et al., 2018). For future development, these can be implemented to explore the effects on predicting SSST due to the variability of water optical properties in inland channels, estuary, nearshore, and offshore.

(b) The skin-cooling anomaly given by SS94 can be noticeably different from that given by S67 and S67m. The SS94 scheme uses three empirical parameters, Λ_0, Rf_{cr} and Ke_{cr}. Their values are currently hardwired into subroutine *oskinsst*, but obviously can vary. For instance, Soloviev and Schlüssel

(1994) suggested $\Lambda_0 = 13.3$ and $\mathsf{Rf}_{cr} = 1.5 \times 10^{-4}$ (which are used in this study), while Soloviev (2007) calibrated $\Lambda_0 = 7.4$ and $\mathsf{Rf}_{cr} = 2 \times 10^{-2}$ using a different dataset and found that with the previously suggested values SS94 underestimated the data considered (in that paper), significantly in light-wind conditions. In future development, we may consider to make these empirical parameters user-specified variables in the input file, providing the flexibility to fine-tune them based on data.

(c) When the warm-layer depth is appropriately specified, the result given by ZB05 can be similar to that by S67m. However, the estimate of warm-layer anomaly can be sensitive to the layer depth specified. In this study, the warm-layer depth z_d is uniformly specified over the entire domain. From the physical point of view, the thickness of warm layer can vary in space, considering the variability of solar heating and wind condition, the movement of sea surface, the bathymetric effects in shallow coastal waters, among other effects. While the ordinary differential equation (10) does not prevent the use of a spatially varying z_d, it lacks the skill to describe the spatial variability of warm layer across the domain; not to mention the challenge to specify such a varying z_d, *a priori*. On the other hand, NCOM resolves the development of warm layer in the upper few meters of depths. With the typical vertical resolution, the NCOM temperature field $T(z)$ gives a reasonable estimate of the warm-layer anomaly. This leads to the issue of possibly double-counting the effect of solar radiation when using ZB05 with the NCOM fields of sufficiently fine vertical resolution. The issue is particularly manifest when a shallower warm-layer depth z_d is specified. In that case, the result of ZB05 leads to patches of abnormally high SSST, since the diurnal fluctuation due to solar heating is presented in the model field $T(z_d)$. In view of this, ZB05 may not be a good option for calculating the SSST when the ocean model resolves the warm-layer structure. But when the model configuration does not have sufficient vertical grids in the upper depths, ZB05 scheme is a viable approach to estimate the warm-layer anomaly, in particular its time evolution.

(d) At present, the effects of skin cooling are not fed into the ocean model integration in a stand-alone NCOM simulation. In a coupled simulation, the NCOM SSST field can be exported as the state of sea surface temperature, thus allowing the effects of skin cooling to be represented in the ocean surface forcing that is determined by the atmospheric model. It is, however, feasible to incorporate the effects of skin cooling into the ocean model dynamics in a stand-alone simulation. A possible approach is to utilize the procedure in option $indsft = indsfs = 5$ in NCOM for setting up ocean surface forcing. This option provides an indirect relaxation of NCOM SST to that would be used in the atmospheric model if a couple simulation were run. This is achieved by computing the latent and sensible heat fluxes from the bulk formula (Kara et al., 2000) using the NCOM SST, together with the input atmospheric data (air temperatures, winds, and humidity) during the run time, while inputing the long-wave heat flux from the data files. Thus, if we use the NCOM SSST field, instead of SST, to compute the latent and sensible heat fluxes in the procedure in option $indsft = indsfs = 5$, this would then mean to indirectly relax NCOM SSST to the state of sea surface temperature that would be exported to the atmospheric model in a coupled simulation.

(e) Further verification tests, against different datasets from independent sources, may be needed to establish the performance metrics of the SSST schemes under various ocean surface conditions. Such information can provide users a guidance in model configuration.

ACKNOWLEDGMENTS

This work is part of the Naval Research Laboratory 6.2 project "Predicting Marine Fog" (PI, Dr. Flagg) funded by the NRL Base Program. We thank Dr. Paul Martin at NRL for discussions on configuring surface forcing in NCOM.

REFERENCES

1. Alappattu, D. P., Wang, Q., Yamaguchi, R., Lind, R. J., Reynolds, M., & Christman, A. J. 2017 Warm layer and cool skin corrections for bulk water temperature measurements for air-sea interaction studies. *J. Geophys. Res. Oceans*, **122**, 6470–6481. https://doi.org/10.1002/2017JC012688.

2. Barron, C. N., & Smedstad, L. F. 2002 Global river inflow with Navy Coastal Ocean Model. *OCEANS '02 MTS/IEEE*, Biloxi, MI. pp 1472–1479. https://doi.org/10.1109/OCEANS.2002.1191855.

3. Donlon, C., Robinson, I., Casey, K. S., Vazquez-Cuervo, J., Armstrong, E., Arino, O., et al. 2007 The global ocean data assimilation experiment high-resolution sea surface temperature pilot project. *Bull. Amer. Meteor. Soc.*, **88**, 1197–1213.

4. Egbert, G. D., Bennett, A. F. & Foreman, M. G. G. 1994 TOPEX/Poseidon tides estimated using a global inverse model. *J. Geophys. Res.*, **99**, 24821–24 852, https://doi.org/10.1029/94JC01894.

5. Egbert, G. D., & Erofeeva, S. Y. 2002 Efficient inverse modeling of barotropic ocean tides. *J. Atmos. Oceanic Technol.*, **19**, 183–204.

6. Fairall, C. W., Bradley, E. F., Godfrey, J. S., Wick, G. A., Edson, J. B., & Young, G. S. 1996a Cool-skin and warm-layer effects on sea surface temperature. *J. Geophys. Res.*, **101**, 1295–1308.

7. Fairall, C. W., Bradley, E. F., Rogers, D. P., Edson, J. B., & Young, G. S. 1996b Bulk parameterization of air-sea fluxes for Tropical Ocean-Global Atmosphere Coupled-Ocean Atmosphere Response Experiment. *J. Geophys. Res.*, **101**, 3747–3764.

8. Grassl, H. 1976 The dependence of the measured cool skin of the ocean on wind stress and total heat flux. *Bound.-Layer Meteor.*, **10**, 465–474.

9. Hasse, L. 1963 On the cooling of the sea surface by evaporation and heat exchange. *Tellus*, **15**, 363–366.

10. Howard, L. N. 1964 Convection at high Rayleigh number. *Proc. the Eleventh Intl. Congress of Applied Mechanics*, Munich, Germany; edited by H. Gortler, Berlin, Springer-Verlag, 1109-1115, 1966.

11. Jerlov, N. G. 1976 *Marine optics*. Elsevier Oceanography Series, Elsevier, Amsterdam.

12. Kara, A.B., Rochford, P. A. & Hurlburt, H. E. 2000 Efficient and accurate bulk parameterizations of air-sea fluxes for use in general circulation models. *J. Atmos. Ocean Tech.*, **17**, 1421–1438.

13. Katsaros, K. B., Liu, T., Businger, J. A. & Tillman, J. E. 1977 Heat transport and thermal structure in the interfacial boundary layer measured in an open tank of water in turbulent free convection. *J. Fluid Mech.*, **83**, 311–335.

14. Liu, T. & Businger, J. A. 1975 Temperature profile in the molecular sublayer near the interface of a fluid in turbulent motion. *Geophys. Res. Lett.*, **2**, 403–404.

15. Mellor, G. L. & Yamada, T. 1982 Development of a turbulent closure model for geophysical fluid problems. *Rev. Geophys.*, **20**, 851–875, https://doi.org/10.1029/RG020i004p00851.

16. Mellor, G. L. 1996 *User's Guide for a Three-Dimensional, Primitive-Equation, Numerical Ocean Model*. Princeton University Press, 39 pp.

17. Metzger, E. J. & Co-authors. 2017 Global Ocean Forecast System 3.1 validation testing. NRL Tech. Rep. NRL/MR/7320–17-9722, 56 pp., https://apps.dtic.mil/sti/citations/AD1034517.

18. Paulson, C. A. & Simpson, J. J. 1981 The temperature difference across the cool skin of the ocean. *J. Geophys. Res.*, **86**, 11044–11054.

19. Pimentel, S., Tse, W.-H., Xu, H., Denaxa, D., Jansen, E., Korres, G., et al. 2019 Modeling the near-surface diurnal cycle of sea surface temperature in the Mediterranean Sea. *J. Geophys. Res. Oceans*, **124**, 171–183. https://doi.org/10.1029/2018JC014289

20. Saunders, P. M. 1967 The temperature at the ocean-air interface. *J. Atmo. Sci.*, **24**, 269–273.

21. Soloviev, A. V. & Schlüssel, P. 1994 Parameterization of the cool skin of the ocean and of the air-ocean gas transfer on the basis of modeling surface renewal. *J. Phys. Oceanogr.*, **24**, 1339–1345.

22. Soloviev, A. V. & Schlüssel, P. 1996 Evolution of cool skin and direct air-sea gas transfer coefficient during daytime. *Bound.-Layer Meteor.*, **77**, 45–68.

23. Verevochkin, Y. G. & Startsev, S. A. 2005 Effect of absorption of solar radiation by water of different optical types on convection and heat transfer just under the air-water interface: The case of zero wind speed. *J. Fluid Mech.*, **523**, 109–120. https://doi.org/10.1017/S0022112004001971

24. Wang, Q. & co-authors. 2018 CASPER: Coupled Air-Sea Processes and Electromagnetic Ducting Research. *Bull. Amer. Meteor. Soc.*, **99**, 1449–1471, doi: 10.1175/BAMS-D-16-0046.1

25. Webster, P. J. & Lukas, R. 1992 TOGA COARE: The coupled ocean–atmosphere response experiment. *Bull. Amer. Meteor. Soc.*, **73**, 1377–1416.

26. Wick, G. A., Emery, W. J., Kantha, L. H. & Schlüessel, P. 1996 The behavior of the bulk – skin sea surface temperature difference under varying wind speed and heat flux. *J. Phys. Oceanogr.*, **26**, 1969–1988.

27. Zeng, X. & Beljaars, A. 2005 A prognostic scheme of sea surface skin temperature for modeling and data assimilation. *Geophys. Res. Lett.*, **32**, L14605.